

Phonon laser in a cavity magnomechanical system

Ming-Song Ding^a, Li Zheng^b, Chong Li^{a,*}

^a*School of Physics, Dalian University of Technology, Dalian 116024, China*

^b*Information Science and Engineering College, Dalian Polytechnic University, Dalian 116034, China*

Abstract

The phonon analog of an optical laser has become the focus of research. We theoretically study phonon laser in a cavity magnomechanical system, which consist of a microwave cavity, a small ferromagnetic sphere and an uniform external bias magnetic field. This system can realize the phonon-magnon coupling and the cavity photon-magnon coupling via magnetostrictive interaction and magnetic dipole interaction respectively, the magnons are driven directly by a strong microwave field simultaneously. First, the intensity of driving magnetic field which can reach the threshold condition of phonon laser is given. Then, we demonstrate that the phonon laser can be well controlled by an adjustable external magnetic field without changing other parameters, which provides an additional degree of freedom compared to the phonon laser in optomechanical systems. Finally, with the experimentally feasible parameters, threshold power in our scheme is close to the case of optomechanical systems. Our results provide a theoretical basis for the realization of phonon lasers in magnomechanical systems.

1. Introduction

In recent years, cavity magnomechanical system has been becoming a novel platform for realizing quantum coherence and coupling between magnons, cavity photons and phonons. Among them, the coupling between photons and magnons is realized by the magnetic dipole interaction, and the interaction between magnons and phonons is based on the magnetostrictive force. As we know the traditional optomechanical systems utilize radiation force [1, 2, 4, 3, 5, 6, 7, 8, 9, 10, 11, 12, 13, 14, 15, 16], electrostatic force [18, 19], and piezoelectric force [20] for coupling phonon with optical or microwave photons, but they all intrinsically lack good tunability. The emergence of magnetostrictive force provides us with a new way to achieve different information carriers [21, 22]. And the highly polished single-crystal yttrium iron garnet (YIG) sphere is introduced into the cavity magnomechanical system as an effective mechanical resonator, the magnons inside it are collective excitation of magnetization, whose frequency can be easily adjusted by external bias magnetic field. The varying magnetization caused by the excitation of the magneton in the YIG sphere results in the geometric deformation of the surface, introducing the coupling between magnon and phonon modes.

Due to YIG sphere's high spin density and low damping rate, the Kittel mode [23] (the ferromagnetic resonance mode) in it can strongly[24, 33, 34] to the microwave cavity photons ($g_{ma} > \kappa_a, \kappa_m$) in cavity-magnon systems. In addition, the YIG sphere has rich magnonic nonlinearities and the characteristic of low loss in different information carriers, these excellent properties make it possible to find many interesting and important phenomena in cavity-magnon systems and cavity magnomechanical systems. Based on it, a lot of theoretical and

experimental researches have been done. J. Q. You *et al.* have found the bistability of cavity magnon polaritons [25], G. S. Agarwal *et al.* have discussed the tripartite entanglement among magnons, cavity photons, and phonons[21]. Furthermore, high-order sideband generation [27, 28], magnon Kerr effect [26], the light transmission in cavity-magnon system [29] and other researches were also studied [30, 31, 32, 33, 34, 35, 36, 58].

Phonon laser as a novel laser has been developed rapidly, it generates coherent sound oscillations (mechanical vibration) by optical pumping. Just like traditional optical laser [37, 38], phonon laser can be considered as an analogue of a two-level optical laser which is provided by phonon mediated transitions between two optical supermodes [39, 40, 41]. These supermodes correspond to the ground and excited states respectively, and the mechanical mode (phonons) mediates the transition between them. As early as 2003, Chen. J and Khurgin have verified the feasibility of phonon lasers and proposed a scheme to realize phonon lasers [42]. Then single trapped ions and quantum dots have been utilized in the fields of phonon laser [43, 44, 45]. Up to now, numerous theoretical and experimental researches have been proposed, such like the cavity optomechanics-based ultralow-threshold phonon lasers [39], the \mathcal{PT} -symmetric phonon laser with balanced gain and loss [40], the nonreciprocal phonon lasing in a coupled cavity system [41], the phonon laser operating at an exceptional point [46], the scheme of amplifying phonon laser by using phonon stimulated emission coherence [47], the phonon-stimulated emission in cryogenic ionic compounds [48, 49], semiconductor superlattices [50] and so on [51, 52, 53, 54]. In addition, phonon laser have also attracted extensive interest in medical imaging and high-precision measurement equipment.

In this work, we study a cavity magnomechanical system, which consist of a microwave cavity, a YIG sphere and the uniform external bias magnetic field H (vertical direction). The

*Corresponding author

Email address: lichong@dlut.edu.com (Chong Li)

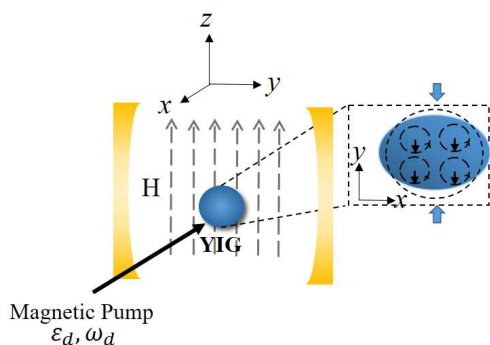


Fig. 1: (1) Schematic illustration of the system, a YIG sphere is placed in the maximum magnetic field of a microwave cavity mode. And an uniform external bias magnetic field H is applied along the z -direction to bias the YIG sphere. The enlarged YIG sphere on the right illustrates how the dynamic magnetization of magnon (vertical black arrows) causes the deformation (compression along the y -direction) of the YIG sphere (and vice versa), which rotates at the magnon frequency. Furthermore, a microwave source is used to drive the magnon mode. It's important to note that the bias magnetic field (z direction), the drive magnetic field (y direction), and the magnetic field (x direction) of the cavity mode are mutually perpendicular at the site of the YIG sphere.

magnetostrictive (radiation pressure like) interaction mediates the coupling between magnons and phonons, and the photons and magnons are coupled via magnetic dipole interaction. It is worth noting that unlike optical pump in the traditional cavity optomechanical system, we introduce magnetic driving field to realize phonon laser. Furthermore, the magnomechanical interaction which is quite weak in experiments can be enhanced by the gain of magnon mode. We found that the production of laser can be well modulated by adjusting the applied magnetic field H , which provides an additional degree of freedom to control phonon laser action. It is worth mentioning that the applied magnetic field H , the drive magnetic field, and the magnetic field of the cavity mode are mutually perpendicular at the site of the YIG sphere. So we can adjust only one of them without worrying about the impact on the rest. Then, the threshold conditions of driving magnetic field intensity for phonon laser is given. We can make our system reach the threshold condition by enhancing drive magnetic field. And the threshold power required can be below $10\mu\text{W}$ within the experimental allowable range of parameters. According to the recent work, the threshold power in cavity optomechanical system is generally about $7\mu\text{W}$ [39, 40, 41]. Accordingly, phonon laser has potential application value in cavity magnomechanical systems.

2. Model and dynamical equations

We consider a hybrid cavity magnomechanical system, which consists a microwave cavity and a small sphere (a highly polished single-crystal YIG sphere of diameter 1mm is used in [26]). There are three modes in this system: cavity photon mode, magnon mode and phonon mode. As shown in Fig. 1, the YIG sphere is placed near the maximum microwave magnetic field of the cavity mode, an uniform external bias magnetic field H is applied along the z direction to bias the YIG sphere simultaneously, which establish the magnon-photon coupling

[26, 25]. The magnon-photon coupling can be tuned by moving the YIG sphere inside the cavity. In addition, the magnetic field H is created by a high precision tunable electromagnet, and the adjusting range of bias magnetic field H is between 0 and 1T [26].

Here, the coupling between magnons and phonons is generated by magnetostrictive interaction (the derivation of the relevant Hamiltonian can be found in [22]). Because of the varying magnetization induced by the magnon excitation inside the YIG sphere, the sphere produce micro deformation and it can be used as an excellent mechanical resonator. Based on it, we have the vibrational modes (phonons) of the sphere. Here, a microwave source is used to directly drive the magnon mode and it can enhance the magnomechanical coupling [26, 21]. It is worth mentioning that the applied magnetic field H , the drive magnetic field, and the magnetic field of the cavity mode are mutually perpendicular at the site of the YIG sphere. So we can adjust only one of them without worrying about the impact on the rest. Furthermore, we concurrently assume that the size of the sphere is so smaller than the wavelength that the interaction between cavity microwave photons and phonons can be neglected. The total Hamiltonian of the hybrid system reads ($\hbar = 1$)

$$\begin{aligned}
 H_{total} &= H_0 + H_{int} + H_d, \\
 H_0 &= \omega_a a^\dagger a + \omega_m m^\dagger m + \omega_b b^\dagger b, \\
 H_{int} &= g_{ma}(a^\dagger m + m^\dagger a) - g_{mb} m^\dagger m (b + b^\dagger), \\
 H_d &= i(\varepsilon_d m^\dagger e^{-i\omega_d t} - \varepsilon_d^* m e^{i\omega_d t}),
 \end{aligned} \tag{1}$$

where H_0 is the free Hamiltonian, the first and second terms denote the cavity photon mode and magnon mode, respectively. The third term describes the mechanical mode. ω_a , ω_m and ω_b denote the resonance frequencies of the cavity, magnon, and mechanical modes. Here, ω_m is the frequency the Kittel mode. An uniform magnon mode resonates in the YIG sphere at frequency $\omega_m = \gamma_g H$, where γ_g is gyromagnetic ratio and $\gamma_g/2\pi = 28\text{GHz/T}$. The annihilation (creation) operators of these modes are $a(a^\dagger)$, $m(m^\dagger)$ and $b(b^\dagger)$, respectively.

H_{int} is the interaction Hamiltonian of system, the first term of H_{int} is the coupling between the cavity and magnon modes, the second term represents phonon-magnon interaction. g_{ma} and g_{mb} are the coupling rates of the magnon-cavity interaction and the magnon-phonon interaction, respectively. And we can tune g_{ma} by adjusting the direction of bias field or the position of the YIG sphere inside the cavity. Finally, H_d is the Hamiltonian which describes the external driving of the magnon mode, as shown in [26], J. Q. You *et al* designed an experimental setup, the YIG sphere can be directly driven by a superconducting microwave line which is connected to the external port of the cavity. Rabi frequency $\varepsilon_d = \frac{\sqrt{5}}{4}\gamma_g \sqrt{M}B_0$ (under the assumption of the low-lying excitations) stands for the coupling strength of the drive magnetic field [21], the amplitude and frequency are B_0 and ω_d respectively. The total number of spins $M = \rho V$, where V is the volume of the sphere. Furthermore, $\rho = 4.22 \times 10^{27}\text{m}^{-3}$ is the spin density of the YIG sphere.

By making a frame rotating at the drive frequency ω_d and using rotating-wave approximation, the total Hamiltonian of the system can be rewritten as

$$\begin{aligned} H_{total} = & -\Delta_a a^\dagger a - \Delta_m m^\dagger m + \omega_b b^\dagger b + \\ & g_{ma}(a^\dagger m + m^\dagger a) - g_{mb} m^\dagger m(b + b^\dagger) \\ & + i(\varepsilon_d m^\dagger - \varepsilon_d^* m), \end{aligned} \quad (2)$$

where $\Delta_a = \omega_d - \omega_a$ is the detuning between the driving field and cavity mode, $\Delta_m = \omega_d - \omega_m$ denotes the detuning between the driving field and resonance frequency of cavity mode. The Heisenberg-Langevin equations of the system are given by

$$\begin{aligned} \dot{a} &= (i\Delta_a - \kappa_a)a - ig_{ma}m - \sqrt{2\kappa_a}a_{int}, \\ \dot{m} &= (i\Delta_m - \kappa_m)m - ig_{ma}a + ig_{mb}m(b + b^\dagger) \\ &+ \varepsilon_d - \sqrt{2\kappa_m}m_{int}, \\ \dot{b} &= (-i\omega_b - \gamma_b)b + ig_{mb}m^\dagger m - \xi_{no}, \end{aligned} \quad (3)$$

where γ_b is the mechanical decay rate, a_{int} , m_{int} and ξ_{no} are input noise operators of cavity, magnon and mechanical modes respectively. κ_m and κ_a are the losses of magnon and microwave cavity modes. Like the computation process of phonon laser [39, 41], assuming that the magnon mode is strongly driven, leading to a large amplitude $|\langle m \rangle| \gg 1$ at the steady state, and due to the cavity-magnon beam splitter interaction, the cavity field also has a large amplitude $|\langle a \rangle| \gg 1$. That leads to the quantum noise terms can be safely neglected if one is interested only in the mean-number behaviors (i.e., the threshold feature of the mechanical gain or the phonon amplifications). Therefore, the semi-classical Langevin equations of motion are used. In other words, we can rewritten all operators as their respective expectation values. Then by setting the left-hand side equal to zero, the steady-state mean values of the system read

$$\begin{aligned} a_s &= \frac{g_{ma} \cdot m_s}{\Delta_a - i\kappa_a}, \\ m_s &= \frac{\varepsilon_d}{(\kappa_m - \frac{g_{ma}^2 \Delta_a}{\Delta_a^2 - \kappa_a^2}) - i[\Delta_m + g_{mb}(b_s + b_s^*) + \frac{g_{ma}^2 \kappa_a}{\Delta_a^2 - \kappa_a^2}]}, \\ b_s &= \frac{g_{mb} |m_s|^2}{\omega_b - i\gamma_b}. \end{aligned} \quad (4)$$

According to the feasible experimental parameters ($g_{mb} < 1\text{Hz}$), $g_{mb}(b_s + b_s^*) \ll \Delta_m$. Under this condition, we approximately have $\Delta_m + g_{mb}(b_s + b_s^*) \sim \Delta_m$. In close analogy to an optical laser, a coherent emission of phonons can be achieved with two coupled whispering-gallery-mode microtoroid resonators via inversion of the two optical supermodes. This leads to phenomenon of phonon laser at the breathing mode, with the threshold power $P_{th} \sim 7\mu\text{W}$ [39, 56]. Similarly, our system also has two supermodes corresponding to the ground and excited states of the two-level system, respectively. The mechanical mode (phonon) can realize energy level transition between levels, the stimulated emission of phonon can be generated by virtue of

magnetic pumping of the upper level, then leading to the appearance of coherent phonon lasing. Therefore we introduce supermode operators $\mathfrak{R}_\pm = (a \pm m^\dagger)/\sqrt{2}$ to rewrite the Hamiltonian H_0 and H_d of the system, i.e.,

$$\begin{aligned} H_{0,sm} &= \omega_+ \mathfrak{R}_+^\dagger \mathfrak{R}_+ + \omega_- \mathfrak{R}_-^\dagger \mathfrak{R}_- + \omega_b b^\dagger b, \\ H_{d,sm} &= i/\sqrt{2}[\varepsilon_d(\mathfrak{R}_+^\dagger + \mathfrak{R}_-^\dagger) - \varepsilon_d^*(\mathfrak{R}_+ + \mathfrak{R}_-)], \end{aligned} \quad (5)$$

where the supermode frequencies $\omega_\pm = -\frac{\Delta}{2} \pm g_{ma}$. H_{int} in Eq.(1) can be transformed to

$$H_{int} = -\frac{g_{mb}}{2}[(n_+ + n_-) + (\mathfrak{R}_+^\dagger \mathfrak{R}_- + \mathfrak{R}_+ \mathfrak{R}_-^\dagger)](b + b^\dagger), \quad (6)$$

with $n_+ = \mathfrak{R}_+^\dagger \mathfrak{R}_+$ and $n_- = \mathfrak{R}_-^\dagger \mathfrak{R}_-$. In the frame rotating with respect to $H_{0,sm}$ and applying the rotating-wave approximation, H_{int} is rewritten as

$$H_{int,sm} = -\frac{g_{mb}}{2}(p^\dagger b + pb^\dagger), \quad (7)$$

where $\hat{p} = \mathfrak{R}_+ \mathfrak{R}_-^\dagger$ is ladder operator. Eq.(7) represents the absorption and emission of phonons. In general, the introduction of supermode operators \mathfrak{R}_\pm means that the magnon mode and the optical mode have the same resonant frequency. After changing the Hamiltonian into the supermode picture, the equations of motion read

$$\begin{aligned} \dot{\mathfrak{R}}_+ &= -(i\omega_+ + \gamma)\mathfrak{R}_+ + \frac{i}{2}g_{mb}b\mathfrak{R}_- + \frac{\varepsilon_d}{\sqrt{2}}, \\ \dot{\mathfrak{R}}_- &= -(i\omega_- + \gamma)\mathfrak{R}_- + \frac{i}{2}g_{mb}b^\dagger\mathfrak{R}_+ + \frac{\varepsilon_d}{\sqrt{2}}, \\ \dot{b} &= -(i\omega_b + \gamma_b)b + \frac{i}{2}g_{mb}p, \\ \dot{p} &= -2(\gamma + ig_{ma})p - \frac{i}{2}g_{mb}b\Delta n + \frac{1}{\sqrt{2}}(\varepsilon_d\mathfrak{R}_-^\dagger + \varepsilon_d^*\mathfrak{R}_+), \end{aligned} \quad (8)$$

where $\gamma = (\kappa_a + \kappa_m)/2$, and $\Delta n = n_+ - n_-$ is inversion operator. Then we set the left-hand side of Eq.(8) equal to zero, the zero-order steady states of the system are given by

$$\begin{aligned} \mathfrak{R}_{+,s} &= \frac{\sqrt{2}\varepsilon_d[2r + i(2\omega_- + bg_{mb})]}{4(\gamma^2 + g_{ma}^2) - \Delta^2 + g_{mb}^2 b^\dagger b - 4i\gamma\Delta}, \\ \mathfrak{R}_{-,s} &= \frac{\sqrt{2}\varepsilon_d[2r + i(2\omega_+ + b^\dagger g_{mb})]}{4(\gamma^2 + g_{ma}^2) - \Delta^2 + g_{mb}^2 b^\dagger b - 4i\gamma\Delta}, \\ p &= \frac{\sqrt{2}((\varepsilon_d \hat{a}_-^\dagger + \varepsilon_d^* \hat{a}_+) - ig_{mb}b\Delta n)}{4\gamma + i(4g_{ma} - 2\omega_b)}, \end{aligned} \quad (9)$$

where $\Delta = \Delta_m + \Delta_a$, then Eq.(9) is substituted into the dynamical equation of b in Eq.(8), the result can be obtained

$$\dot{b} = \Delta_b b + \chi, \quad (10)$$

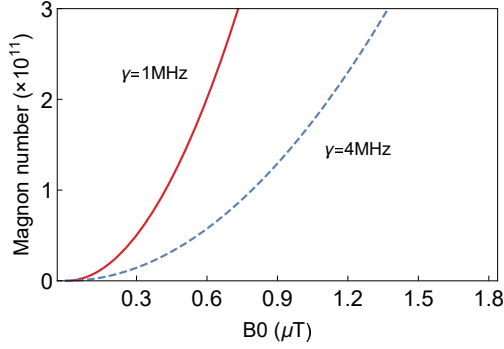


Fig. 2: The distribution of steady-state magnon number $|m_s|^2$ versus the drive magnetic field B_0 under $\gamma = 1\text{MHz}$ (red solid line) and $\gamma = 4\text{MHz}$ (blue dashed line). The parameter we used is $\Delta_m/2\pi = 8\text{MHz}$.

with

$$\begin{aligned}\Delta_b &= -i\omega'_b - G - \gamma_b, \\ G &= g_{mb}^2\gamma\left[\frac{\Delta n}{8\gamma^2 + 2\eta^2} + \beta\right], \\ \beta &\simeq \frac{|\varepsilon_d|^2 \eta \Delta}{4(\gamma^2 + g_{ma}^2 - \frac{\Delta^2}{4} + \Delta^2\gamma^2)(\eta + 4\gamma^2)},\end{aligned}\quad (11)$$

where $\eta = 2g_{ma} - \omega_b$, and the approximation is due to the parameters we have chosen ($g_{mb} \ll \Delta$). Then the inversion operator can be expressed as

$$\Delta n \simeq \frac{2g_{ma}|\varepsilon_d|^2}{(\gamma^2 + g_{ma}^2 - \frac{\Delta^2}{4})^2 + \gamma^2\Delta^2}.\quad (12)$$

Because this paper mainly studies the phonon laser generated by the system, we are only interested in G , which indicates the mechanical gain of the system. Therefore, only the specific expression of G is given. The non-negative mechanical gain G decreases the effective damping rate of the mechanical mode $\gamma_{eff} = \gamma_b - G$, that leads to the instabilities of the mechanical oscillator at $\gamma_{eff} < 0$. This problem has been analyzed and discussed in [39, 41, 55] from both theoretical and experimental perspectives.

3. The distribution of steady-state magnon number

Here, we give the specific values of the parameters used in this paper [22]. $\omega_a/2\pi = \omega_m/2\pi = 10.1\text{GHz}$, $\omega_b/2\pi = 12\text{MHz}$, $g_{ma}/2\pi = 6\text{MHz}$, $g_{mb}/2\pi = 0.1\text{Hz}$, $\Delta_a/2\pi = 8\text{MHz}$, and the loss of mechanical modes $\gamma_b/2\pi = 100\text{Hz}$. Our research is in the resolved sideband regime ($\kappa_m/\omega_b < 1$). The drive power $P = (B_0^2/2\mu_0)Ac$ [21], where $B_0^2/2\mu_0$ is the time average of energy per unit volume, c is the speed of an electromagnetic wave propagating through the vacuum and A is the maximum cross-sectional area of the YIG sphere. Fig. 2 shows the distribution of steady-state magnon number $|m_s|^2$ versus the drive magnetic field B_0 . The number of magnons increases exponentially with the increase of B_0 , which represents significant nonlinearity. The corresponding B_0 is much weaker relative to the external magnetic field H . In addition, the results under different losses

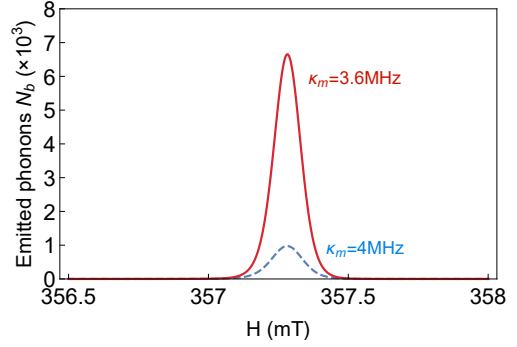


Fig. 3: The stimulated emitted phonon number n_b versus the external bias magnetic field H under $\kappa_m = 3.6\text{MHz}$ (red solid line) and $\kappa_m = 4\text{MHz}$ (blue dashed line). The parameter we used is $\varepsilon_d = 1.45 \times 10^{11}\text{Hz}$ ($B_0 = 2\mu\text{T}$, $P = 23\mu\text{W}$) and $\kappa_a = 3\text{MHz}$.

of supermode γ are also given. It can be seen that the smaller the dissipation, the faster $|m_s|^2$ increases.

4. Magnetic field-based control of phonon laser action

In order to explore the relationship between the generation of phonon laser and magnetic field (including the external bias magnetic field H and the drive magnetic field B_0), we investigate the phonon number as a function of H and B_0 . The mechanical gain G has been given in Eq.(11), thus the stimulated emitted phonon number can be calculated [40, 41], i.e.,

$$N_b = \exp[2(G - \gamma_b)/\gamma_b],\quad (13)$$

then from the above expression, the threshold condition of phonon laser is given (the threshold condition for phonon lasing $N_b = 1$). When $N_b = 1$, we have

$$B_{0,th} = \frac{8\sqrt{\frac{2}{5}}\gamma_b\Gamma}{g_{mb}\sqrt{g_{ma}M\gamma\Delta}},\quad (14)$$

where $\Gamma = g_{ma}^4 + 2g_{ma}^2(\gamma^2 - \frac{\Delta^2}{4}) + (\gamma^2 + \frac{\Delta^2}{4})^2$. $B_{0,th}$ is the driving magnetic field required to achieve the threshold condition of the phonon laser in our system. Finally, according to the expression given earlier $P = (B_0^2/2\mu_0)Ac$, the threshold power is defined as

$$P_{th} = \frac{64}{5} \frac{Ac\gamma_b\Gamma}{g_{mb}^2g_{ma}M\gamma\mu_0\Delta}.\quad (15)$$

In Fig. 3, N_b is plotted as a function of the external bias magnetic field H . There is an obvious window between $H \approx 357\text{mT} - 357.5\text{mT}$ which generates a large number of stimulated emitted phonons. This behavior is consistent with the previous effect on the number of magnons, and the reason for it is the cavity-magnon beam splitter interaction. We find that the distribution of the stimulated emitted phonon number has a Lorentzian-like shape dependence on the applied magnetic field H , which presents an additional degree of freedom to control the phonon laser. And that phenomenon similar to a switch of a phonon laser can be obtained by adjusting H without changing other parameters. Especially, the widths of the windows almost

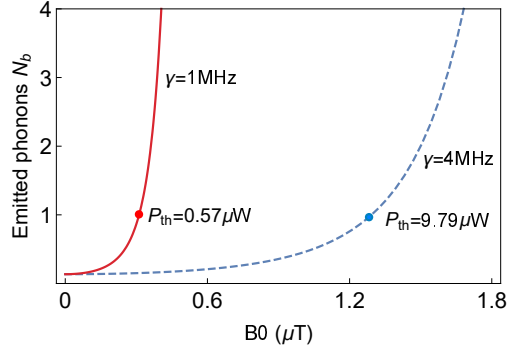


Fig. 4: The stimulated emitted phonon number n_b versus the drive magnetic field B_0 under $\kappa_m = \kappa_a = 1\text{MHz}$ (red solid line, $P_{th} = 0.57\mu\text{W}$) and $\kappa_m = \kappa_a = 4\text{MHz}$ (blue dashed line, $P_{th} = 9.79\mu\text{W}$). The other parameter we used is $\Delta_m/2\pi = 8\text{MHz}$.

keep unchanged with the loss of magnon mode κ_m . Moreover, it can be seen that the number of phonons increases with decreasing κ_m .

In Fig. 4, N_b is plotted as a function of the drive magnetic field B_0 , the stimulated emitted phonon number is enhanced by input driving magnetic field. Note that the threshold condition of phonon laser can be reached at $N_b \geq 1$. Then we find the loss of supermode has significant impact on the threshold power P_{th} . For $\gamma = 1\text{MHz}$ and $\gamma = 4\text{MHz}$, we have $P_{th} \sim 0.57\mu\text{W}$ and $P_{th} \sim 9.79\mu\text{W}$, respectively. It is worth mentioning that P_{th} is calculated in the range of parameters that can be achieved by experiments, and it is not much different from the P_{th} obtained in the cavity optomechanics system, and the threshold power in cavity optomechanical system is generally about $7\mu\text{W}$ in [39, 40, 41, 57].

5. Conclusion

In summary, we have investigated theoretically phonon laser in a hybrid cavity magnomechanical system, which use magnetostrictive force (radiation pressure like) to achieve interaction between magnon mode and mechanical mode. Our results have shown that by adjusting the the external bias magnetic field H , a window which generates a large number of phonons can be obtained. And the width of this window is about 0.5mT . Compared with the conventional phonon laser work [39, 40, 41], our scheme provides an additional degree of freedom to control phonon laser action.

We first consider a novel drive magnetic field, which can be realized by directly driving the YIG sphere with a microwave source. The threshold conditions of driving magnetic field intensity for phonon laser is given. Then, we find the system can reach the threshold power and produce phonon laser by increasing the drive magnetic field B_0 . With the experimentally feasible parameters, threshold power P_{th} in our system is close to the threshold power of phonon laser in optomechanical systems which are mature in theory and experiments. Finally, we hope that the phonon laser in the hybrid cavity magnomechanical system will be accessible in the near future.

6. acknowledgments

This work was supported by the National Natural Science Foundation of China, under Grant No. 11574041 and No. 11475037.

References

- [1] Aspelmeyer, M., Kippenberg, T. J. & Marquardt, F. Cavity optomechanics. *Rev. Mod. Phys.* **86**, 1391 (2014).
- [2] Li, M. et al. Harnessing optical forces in integrated photonic circuits. *Nature* **456**, 480 (2008).
- [3] Safavi-Naeini, A. H. et al. Electromagnetically induced transparency and slow light with optomechanics. *Nature* **472**, 69 (2011).
- [4] Huang, J. G. et al. A dissipative self-sustained optomechanical resonator on a silicon chip. *Appl. Phys. Lett.* **112**, 051104 (2018).
- [5] Vovrosh, J. et al. Parametric feedback cooling of levitated optomechanics in a parabolic mirror trap. *J. Opt. Soc. Am. B.* **34**, 1421-1428 (2017).
- [6] Zhang, X. Y., Zhou, Y. H., Guo, Y. Q. & Yi, X. X. Double optomechanically induced transparency and absorption in parity-time-symmetric optomechanical systems. *Phys. Rev. A* **98**, 033832 (2018).
- [7] Wu, Q., Zhang, J. Q., Wu, J. H., Feng, M. & Zhang, Z. M. Tunable multi-channel inverse optomechanically induced transparency and its applications. *Opt. Express* **23**, 18534 (2015).
- [8] Xiong, B., Li, X., Chao, S. L. & Zhou, L. Optomechanical quadrature squeezing in the non-Markovian regime. *Opt. Lett.* **43**, 6053-6056 (2018).
- [9] Li, W., Li, C. & Song, H. Quantum synchronization in an optomechanical system based on Lyapunov control. *Phys. Rev. E* **93**, 06222 (2016).
- [10] Rabl, P. Photon blockade effect in optomechanical systems. *Phys. Rev. Lett.* **107**, 063601 (2011).
- [11] Heinrich, G., Ludwig, M., Qian, J., Kubala, B. & Marquardt, F. Collective dynamics in optomechanical arrays. *Phys. Rev. Lett.* **107**, 043603 (2011).
- [12] Purdy, T. P., Yu, P. L., Peterson, R. W., Kampel, N. S. & Regal, C. A. Strong optomechanical squeezing of light. *Phys. Rev. X* **3**, 031012 (2013).
- [13] Liao, J. Q. & Nori, F. Photon blockade in quadratically coupled optomechanical systems. *Phys. Rev. A* **88**, 023853 (2013).
- [14] Zeng, Y. X., Gebremariam, T., Ding, M. S. & Li, C. Quantum optical diode based on Lyapunov control in a superconducting system. *J. Opt. Soc. Am. B.* **35**, 2334 (2018).
- [15] Li, J., Li, G., Zippilli, S., Vitali, D. & Zhang, T. Enhanced entanglement of two different mechanical resonators via coherent feedback. *Phys. Rev. A* **95**, 043819 (2017).
- [16] Gao, Y. P. et al. Effective mass sensing using optomechanically induced transparency in microresonator system. *IEEE Photonics J.* **9**, 1-11 (2016).
- [17] Liu, X. F., Wang, T. J. & Wang, C. Optothermal control of gains in erbium-doped whispering-gallery microresonators. *Opt. Lett.* **43**, 326-329 (2018).
- [18] Andrews, R.W. et al. Bidirectional and efficient conversion between microwave and optical light. *Nat. Phys.* **10**, 321-326 (2014).
- [19] Bagci, T. et al. Optical detection of radio waves through a nanomechanical transducer. *Nature* **507**, 81-85 (2014).
- [20] Fan, L., Fong, K. Y., Poot, M. & Tang, H. X. Cascaded optical transparency in multimode-cavity optomechanical systems *Nat. Commun.* **6**, 5850 (2015).
- [21] Li, J., Zhu, S. Y. & Agarwal, G. S. Magnon-photon-phonon entanglement in cavity magnomechanics. *Phys. Rev. Lett.* **121**, 203601 (2018).
- [22] Zhang, X., Zou, C. L., Jiang, L. & Tang, H. X. Cavity magnomechanics. *Sci. Adv.* **2**, e1501286 (2016).
- [23] Kittel, C. On the theory of ferromagnetic resonance absorption. *Phys. Rev.* **73**, 155 (1948).
- [24] Huebl, H. et al. High cooperativity in coupled microwave resonator ferromagnetic insulator hybrids. *Phys. Rev. Lett.* **111**, 127003 (2013).
- [25] Wang, Y. P. et al. Bistability of Cavity Magnon Polaritons. *Phys. Rev. Lett.* **120**, 057202 (2018).
- [26] Wang, Y. P. et al. Magnon Kerr effect in a strongly coupled cavity-magnon system. *Phys. Rev. B* **94**, 224410 (2016).
- [27] Liu, Z. X., Wang, B., Xiong, H. & Wu, Y. Magnon-induced high-order sideband generation. *Opt. Lett.* **43**, 3698 (2018).
- [28] Xiong, X. R. et al. The analysis of high-order sideband signals in optomechanical system. *Sci. China. Phys. Mech.* **61**, 90322 (2018)

- [29] Wang, B., Liu, Z. X., Kong, C., Xiong, H. & Wu, Y. Magnon-induced transparency and amplification in PT-symmetric cavity-magnon system. *Opt. Express* **26**, 20248-20257 (2018).
- [30] Woods, L. M. Magnon-phonon effects in ferromagnetic manganites. *Phys. Rev. B* **65**, 014409 (2001).
- [31] Kalashnikova, A. M. et al. Impulsive excitation of coherent magnons and phonons by subpicosecond laser pulses in the weak ferromagnet FeBO₃. *Phys. Rev. B* **78**, 104301 (2008).
- [32] Gao, Y. P., Cao, C., Wang, T. J., Zhang, Y. & Wang, C. Cavity-mediated coupling of phonons and magnons. *Phys. Rev. A* **96**, 023826 (2017).
- [33] Zhang, X., Zou, C. L., Jiang, L. & Tang, H. X. Strongly coupled magnons and cavity microwave photons. *Phys. Rev. Lett.* **113**, 156401 (2014).
- [34] Bai, L. et al. Spin Pumping in Electrodynamically Coupled Magnon-Photon Systems. *Phys. Rev. Lett.* **114**, 227201 (2015).
- [35] Goryachev, M. et al. High-cooperativity cavity QED with magnons at microwave frequencies. *Phys. Rev. Applied* **2**, 054002 (2014).
- [36] Cao, C. et al. Tunable high-order sideband spectra generation using a photonic molecule optomechanical system. *Sci. Rep.* **6**, 22920 (2016).
- [37] Bonifacio, R. & De Salvo, L. Collective atomic recoil laser (CARL) optical gain without inversion by collective atomic recoil and self-bunching of two-level atoms. *Nucl. Instrum. Method Phys. Res. Sect. A* **341**, 360 (1994).
- [38] Gauthier, D. J., Wu, Q., Morin, S. E. & Mossberg, T. W. Realization of a continuous-wave, two-photon optical laser. *Phys. Rev. Lett.* **68**, 464 (1992).
- [39] Grudinin, I. S., Lee, H., Painter, O. & Vahala, K. J. "Phonon laser action in a tunable two-level system," *Phys. Rev. Lett.* **104**, 083901 (2010).
- [40] Jiang, Y. et al. PT-Symmetric Phonon Laser. *Phys. Rev. Lett.* **113**, 053604 (2014).
- [41] Jiang, Y. et al. Nonreciprocal Phonon Laser. *Phys. Rev. Applied* **10**, 064037 (2018).
- [42] Chen, J. & Khurgin, J. B. Feasibility analysis of phonon lasers. *IEEE. J. Quantum. Elect.* **39**, 600 (2003).
- [43] Wallentowitz, S., Vogel, W., Siemers, I. & Toschek, P. E. Vibrational amplification by stimulated emission of radiation. *Phys. Rev. A* **54**, 943 (1996).
- [44] Khaetskii, A., Golovach, V. N., Hu, X. & Žutić, I. Proposal for a phonon laser utilizing quantum-dot spin states. *Phys. Rev. Lett.* **111**, 186601 (2013).
- [45] Kabuss, J., Carmele, A., Brandes, T. & Knorr, A. Optically driven quantum dots as source of coherent cavity phonons: a proposal for a phonon laser scheme. *Phys. Rev. Lett.* **109**, 054301 (2012).
- [46] Zhang, J. et al. A phonon laser operating at an exceptional point. *Nat. Photonics* **12**, 479 (2018).
- [47] Mahboob, I., Nishiguchi, K., Fujiwara, A. & Yamaguchi, H. Phonon lasing in an electromechanical resonator. *Phys. Rev. Lett.* **110**, 127202 (2013).
- [48] Fokker, P. A., Dijkhuis, J. I. & De Wijn, H. W. Stimulated emission of phonons in an acoustical cavity. *Phys. Rev. B* **55**, 2925 (1997).
- [49] Bron, W. E. & Grill, W. Stimulated phonon emission. *Phys. Rev. Lett.* **40**, 1459 (1978).
- [50] Kent, A. J. et al. Acoustic phonon emission from a weakly coupled superlattice under vertical electron transport: observation of phonon resonance. *Phys. Rev. Lett.* **96**, 215504 (2006).
- [51] Vahala, K. M. et al. A phonon laser. *Nat. Phys.* **5**, 682 (2009).
- [52] He, B., Yang, L. & Xiao, M. Dynamical phonon laser in coupled active-passive microresonators. *Phys. Rev. A* **94**, 031802 (2016).
- [53] Herrmann, M. et al. Injection locking of a trapped-ion phonon laser. *Phys. Rev. Lett.* **105**, 013004 (2010).
- [54] Mahboob, I., Nishiguchi, K., Fujiwara, A. & Yamaguchi, H. Phonon lasing in an electromechanical resonator. *Phys. Rev. Lett.* **110**, 127202 (2013).
- [55] Cohen, J. D. et al. Phonon counting and intensity interferometry of a nanomechanical resonator. *Nature* **520**, 522 (2015).
- [56] Wang, G. et al. Demonstration of an ultra-low-threshold phonon laser with coupled microtoroid resonators in vacuum. *Photon. Res.* **5**, 73 (2017).
- [57] Wang, B. et al. Polarization-based control of phonon laser action in a Parity Time-symmetric optomechanical system. *Commun. Phys.* **43**, 1 (2018).
- [58] Li, J., Zhu, S. Y. & Agarwal, G. S. Squeezed states of magnons and phonons in cavity magnomechanics. *Phys. Rev. A* **99**, 021801 (2019).